A soft robotic total artificial hybrid heart

Maziar Arfaee [1,2,9], Annemijn Vis[2,9], Paul A. A. Bartels[3,4], Lucas C. van Laake [5], Lucrezia Lorenzon [6], Dina M. Ibrahim[3,4], Debora Zrinscak[6], Anthal I. P. M. Smits [3,4], Andreas Henseler[7], Matteo Cianchetti [6], Patricia Y. W. Dankers [3,4,8], Carlijn V. C. Bouten [3,4], Johannes T. B. Overvelde [5] & Jolanda Kluin [1]

End-stage heart failure is a deadly disease. Current total artificial hearts (TAHs) carry high mortality and morbidity and offer low quality of life. To overcome current biocompatibility issues, we propose the concept of a soft robotic, hybrid (pumping power comes from soft robotics, innerlining from the patient's own cells) TAH. The device features a pneumatically driven actuator (septum) between two ventricles and is coated with supramolecular polymeric materials to promote anti-thrombotic and tissue engineering properties. In vitro, the Hybrid Heart pumps 5.7 L/min and mimics the native heart's adaptive function. Proof-of-concept studies in rats and an acute goat model demonstrate the Hybrid Heart's potential for clinical use and improved biocompatibility. This paper presents the first proof-of-concept of a soft, biocompatible TAH by providing a platform using soft robotics and tissue engineering to create new horizons in heart failure and transplantation medicine.

End-stage heart failure has a high mortality rate[1], and while heart transplantation is the best treatment[2], donor hearts are scarce[3]. This limitation has led to the development of total artificial hearts (TAHs) and left ventricular assist devices (LVADs). However, the clinical application of currently available TAHs and LVADs is largely hampered by their poor biocompatibility[4], mainly caused by their non-physiological way of propelling blood and the use of non-autologous materials[5]. These factors can induce thromboembolic complications and bleeding complications due to acquired von Willebrand disease or due to the inherent anticoagulation regimen[6]. Another limitation of the current generation of devices is the use of percutaneous drivelines required for actuation, that carry a high infection risk and significantly impact the patients' quality of life[7]. Due to the high complication rate and low quality of life, the currently clinically available TAHs, SynCardia (SynCardia Systems, Tucson, AZ, USA) and Carmat (Aeson; Carmat, Vélizy-villacoublay, France), are sparsely implanted[8,9].

We hypothesize that a TAH in which the pumping (beating) power comes from soft robotics can propel the blood in a physiological way. Combined with supramolecular coatings to prevent blood clots and integrate with the patient's cells this could then result in a hybrid TAH. Here, we describe the development of the Hybrid Heart as a proof of concept of a soft robotic heart with some biomimetic properties, such as tissue-engineered inner lining, electronics-free control of the heartbeat, and wireless energy transfer. As such, the Hybrid Heart provides a platform to tackle the multiple issues currently associated with TAHs, with the aim to come closer to the ultimate goal of providing destination therapy for end-stage heart failure (Fig. 1).

Results

Rational and design of the hybrid heart

As no TAH is as good as a donor heart[8], we believe that the new generation of TAH should as closely as possible mimic the anatomy and function of the human heart. As the human blood vessels and organs

[1]Department of Cardiothoracic Surgery, Thorax Center, Erasmus MC Rotterdam, Rotterdam, The Netherlands. [2]Department of Cardiothoracic Surgery, Amsterdam UMC location University of Amsterdam, Amsterdam, The Netherlands. [3]Department of Biomedical Engineering, Eindhoven University of Technology, Eindhoven, The Netherlands. [4]Institute for Complex Molecular Systems, Eindhoven University of Technology, Eindhoven, The Netherlands. [5]Autonomous Matter Department, AMOLF, Amsterdam, The Netherlands. [6]The BioRobotics Institute, Scuola Superiore Sant'Anna, Pisa, Italy. [7]Evos GMBH, Merzbrück, Germany. [8]Department of chemical engineering and chemistry, Eindhoven University of Technology, Eindhoven, The Netherlands. [9]These authors contributed equally: Maziar Arfaee, Annemijn Vis. ✉e-mail: j.kluin@erasmusmc.nl
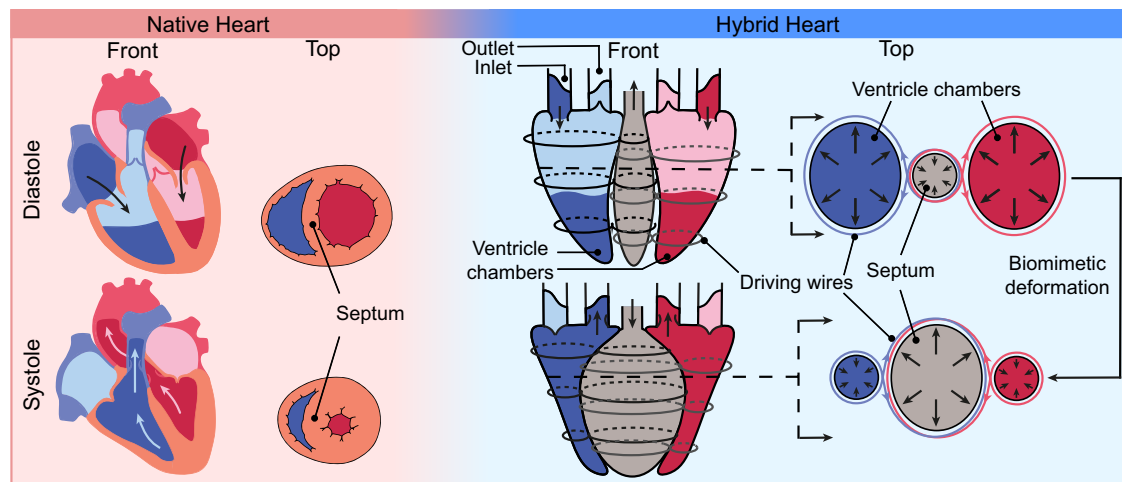
Fig. 1 | The Hybrid Heart design. The Hybrid Heart is a soft robotic, pulsatile TAH that enables a soft contractile motion similar to the human heart. It is actuated by a pneumatic actuator (septum) positioned between the ventricles, surrounded by wires that wrap around both septum and each ventricle in a shape of (∞).

are designed to perform under pulsatile blood flow, pulsatile flow seems to be beneficial over continuous flow in long term[10,11]. In addition, propelling the blood in a physiological way is key in preventing thrombotic complications that are currently seen with LVADs and TAHs. The use of soft materials can create bio-inspired motions[12,13] (including passive Frank-Starling like behavior), and safe interaction with blood and the surrounding tissues[5]. The ideal TAH should therefore be free from any thrombotic complications. The human heart has two blood chambers (ventricles), separated by a septum, that eject blood simultaneously at each heartbeat. During systole, the ventricular walls and the interventricular septum contract synchronously, resulting in ejection of blood from both chambers. The contraction of the septum is responsible for 40% of the left ventricular output and is the major force of ejection for the right ventricular output[14]. To mimic the human heart contraction closely, an ideal TAH should have two ventricles and a working septum that contributes to the cardiac output. In general, a TAH must deliver the same cardiac output as the human heart during resting and performing light activities, which is 5–6 L/min at a heart rate of 60–100/min[15].

Given the importance of the septum in cardiac function, we conceptualized this in the Hybrid Heart design. The Hybrid Heart has two blood collecting chambers like those in the human heart, which we refer to as "ventricles". Both artificial ventricles are similar in shape and size and can hold a maximum volume of 140 ml each. In between the ventricles of the Hybrid Heart, one soft pneumatic muscle is placed, which we refer to as the "septum" with a maximum volume of ~160 ml. The septum is inflated and deflated using relative positive or negative air pressure. Multiple inextensible wires, wrapped around the septum and ventricles in a closed-loop infinity symbol (∞), distribute the forces over the surfaces of both ventricles of the Hybrid Heart (Fig. 1). Importantly, when the septum inflates, its internal diameter increases, and more length of each wire goes around the septum. As the total length of each wire is constant, they squeeze the ventricles, resulting in ejection of fluid from the ventricles (i.e., blood). Moreover, when the septum is pressurized, it also pushes against the ventricular walls attached to it. Note that the length of each wire and the number of wires around each ventricle dictate the stroke volume ejected by the Hybrid Heart. A deflated septum represents diastole, enabling the passive filling of the ventricles (Movie 1). This process is further supported by the native atria, which remain intact just before the inlet valves, functioning similarly to the ventricles in our native heart[16].

Typically, soft robotic devices are fabricated using extensible materials, such as silicones and soft polyurethanes[17,18], as their functionality often relies on their material extensibility. However, the

durability of these materials when stretching them for as much as 3 billion times in a lifetime at frequencies ranging from 60 to 100 Hz, is a major issue. Here, we opted to develop a concept, in which we can also use thin and flexible yet almost inextensible materials, exploring another material type and actuation method, and expanding the library of soft robotic techniques used in implantable applications. Although its improved durability is yet to be confirmed by more studies and also design optimizations to prevent stress concentrations, this approach fundamentally reduces wall stretch as the "softness" originates from bending rather than stretching, thereby creating an optimal condition for in situ tissue engineering. We used nylon with a coating of thermoplastic polyurethane (TPU, 70 den, 170 g/qm, extremtextil, Dresden, Germany) for the ventricles and the septum.

Each ventricle has one inlet and one outlet for blood, which can be fitted with any valve type to direct the blood flow. In this proof of principle, we opted for mechanical heart valves for pragmatic reasons, as they are easy to sanitize and can be stored in a dry stage. The Hybrid Heart weighs 62 g including both ventricles, the pneumatic muscle, wires and four mechanical heart valves (when empty). The length from valves to apex is 11 cm and the maximum width is 10 cm.

In vitro quasi-static experiments

In the in vitro quasi-static experiments, we found that the Hybrid Heart only started to contract after the septum pressure reached a critical value, and only returned to its initial shape at a significantly lower critical value, indicating hysteresis in the mechanical response (Figs. S3–S6). Importantly, this effect mainly originates from mechanical hysteresis intrinsic to the Hybrid Heart design and not from friction between wires and the fabrics, which we concluded from a simplified analytical model (Figs. S7–S9). The hysteresis results in a slow buildup of pressure in the ventricles and leads to a fast actuation and contraction of the ventricles. Note that this slow buildup of pressure inside the ventricles (isovolumetric contraction phase) and rapid increase during contraction resembles the pumping physiology of the human heart[4].

Dynamic test bench performance

Dynamic behavior of the Hybrid Heart was evaluated in a mock circulatory loop (Figs. S11, S12). Figure 2a shows the Hybrid Heart prototype at end-systolic and end-diastolic conditions. We found that, under physiological conditions (Fig. 2b), the left ventricle of the Hybrid Heart has a maximum cardiac output of 5.71 ± 0.04 L/min at 60 beats per minute (bpm) (Fig. 2c). Since a portion of blood ejected by the left ventricle is shunted directly to the left atrium via the bronchial
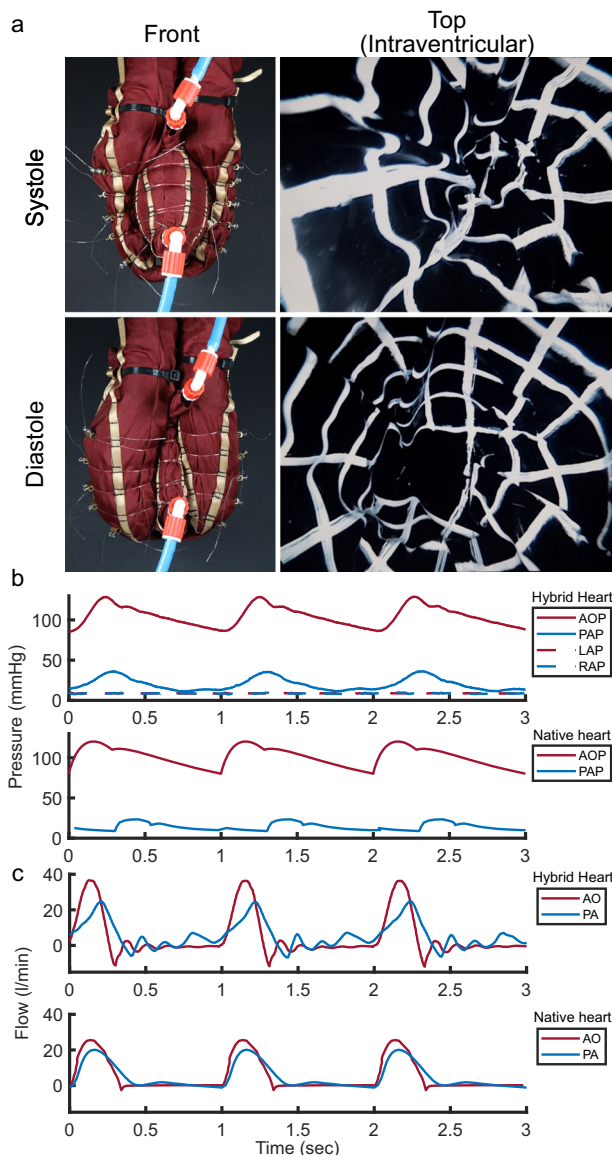
Fig. 2 | In vitro test results of the hybrid heart. All tests were performed in the double mock circulatory loop. **a** Hybrid Heart in front view (left images) and the view inside the ventricle, captured by a laparoscope (right images), during systole and diastole. **b** On top, pressure curves measured during hybrid heart operation in the mock circulatory loop, followed by pressure curves of the native heart below. AOP: aortic pressure, PAP: pulmonary artery pressure, LAP: left atrial pressure, RAP: right atrial pressure. **c** Flow curves measured during hybrid heart operation in the mock circulatory loop, followed by flow curves of native heart below[47,48]. AO: blood flow in aorta, PA: blood flow in pulmonary artery.

circulation[19], higher ventricular outputs of the left ventricle are needed compared to the right ventricle. Therefore, we set the right ventricular output to a lower value of 5.02 ± 0.08 L/min. We were able to decrease the right ventricular output relatively to the left ventricular output by adjusting the length of the wires around the right ventricle.

The human heart automatically balances its cardiac output through the Frank-Starling mechanism[20]. A TAH needs to have a similar mechanism that allows for increased cardiac output when the preload increases, otherwise severe complications such as respiratory failure can occur. Ideally, this mechanism should be passive, to avoid the use of additional hardware and sensors that are often prone to failure[21]. In the Hybrid Heart, we solely use inextensible materials that are inherently non-compliant in comparison to the stiffness of the human heart.

However, in our design the ventricles can be compliant because of their geometry and the compliance of the air in the septum. With the laparoscopic camera, we observed that during contraction, multiple folds and wrinkles are formed in the ventricles (Fig. 2a). In addition, the laparoscopic test (Figs. S24, S25) showed that the ventricles do not completely distend during diastole, allowing for a buffer volume inside the ventricles for increased venous return (preload sensitivity). In case of a rise in venous return, the folds straighten, resulting in an increased stroke volume (Video S5). Preload sensitivity of the left and right ventricles is illustrated in Fig. 3a, b as a function of preload and heart rate. At the heart rates of 60 and 70 bpm, cardiac output seems to increase almost linearly by increasing the preload on both sides. Preload sensitivity of 0.0701 and 0.0894 L/min/mmHg are measured respectively for left and right ventricles at 60 bpm. By increasing the heart rate to 70 bpm, both left and right preload sensitivity decreases slightly to respectively 0.0577 and 0.0674 L/min/mmHg. However, we observe different behavior at higher heart rate of 80 bpm, where we can identify two distinct region of preload sensitivity for right ventricle. From 4 to 8 mmHg, right CO increases from 4.55 L/min to 6.2 L/min, resulting in a preload sensitivity of 0.4354 L/min/mmHg, after which CO remains approximately constant at 6.36 ± 0.07 L/min. A similar trend is observed for left side as well, where the CO of 80 bpm at 4 mmHg is lower than CO at 70 bpm, and increases rapidly by increasing the preload. However left preload sensitivity can be divided into three regions. Firstly, from 4 to 6 mmHg where the Hybrid Heart ejects 0.550 L/min extra for each mmHg of preload rise. Between 6-12 mmHg and 12-20 mmHg, left preload sensitivity decreases to respectively 0.1538 L/min/mmHg and 0.0511 L/min/mmHg. In general, the mean preload sensitivity of the left ventricle is calculated as 0.176 ± 0.213 L/min/mmHg.

Regarding afterload sensitivity, we found that the Hybrid Heart's left ventricle ejects 28 ± 1 mL/min less, for each mmHg afterload rise. As illustrated in Fig. 3c, heart rate has almost no effect on afterload sensitivity of the Hybrid Heart on both sides. The same trend applies to the right-side afterload sensitivity (Fig. 3d). While, it has higher afterload sensitivity by ejecting 104 ± 23 mL/min less, for each mmHg afterload rise. It should be noted that we could not have perfect control over right afterload at higher frequencies due to the limitations of our mock circulatory loop. However, we assumed that it is not affecting the characterization of the afterload sensitivity, as CO decreases quite linearly by increasing the afterload (Fig. 3c, d).

Figure 3e, f demonstrate the ability of the Hybrid Heart to passively adjust the left and right CO in case of acute imbalance in left and right preloads. As shown in Fig. 3e, by increasing right preload from 10 to 16 mmHg, and decreasing left preload from 10 to 4 mmHg, right SV increased dramatically up to 25%, while left SV also decreases 10%, resulting in balancing the preloads after ~60 beats. However, the Hybrid Heart was not able to fully maintain balanced output in reverse scenario, where right preload is decreased from ~10 to 4 mmHg, and left preload is increased from 10 to 15 mmHg (Fig. 3f). This can be due to different preload sensitivity of right and left ventricle in the preloads ranged between 4–16 mmHg at 60 bpm. As illustrated in Fig. 3a, b, right-side preload sensitivity becomes higher at 10–16 mmHg (0.1256 L/min/mmHg) than 4–10 mmHg (0.0734 L/min/mmHg), while on the other side, left-side preload sensitivity is higher at 4–10 mmHg (0.1009 L/min/mmHg) than 10–16 mmHg (0.0504 L/min/mmHg). This can explain the better performance of the Hybrid Heart at 60 BPM, when right preload becomes higher than left preload.

4D flow magnetic resonance imaging results revealed that the flow during the filling and ejection phases of the Hybrid Heart's ventricles is laminar (Supplementary Fig. S13).

Acute animal experiment

As a proof of concept, we assessed the performance of the Hybrid Heart in an acute goat animal model, excluding the use of a
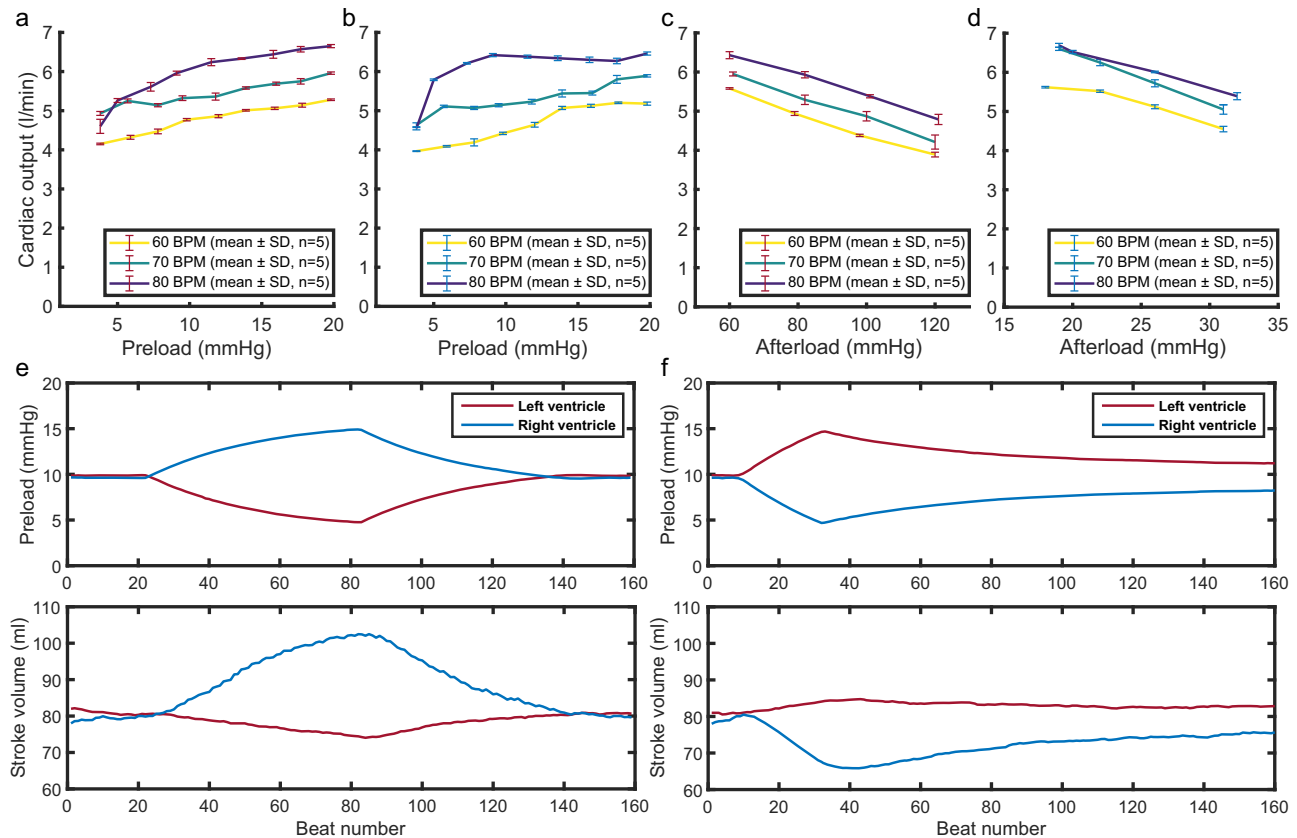
Fig. 3 | In vitro characterization of hybrid heart's preload and afterload sensitivity. All tests were performed in the double mock circulatory loop at different heart rates of 60, 70, and 80 BPM. Data are presented as mean ± SD of $n = 5$ cycles. a) The relation between varying left preload (4-20 mmHg) versus left cardiac output. b) The relation between varying right preload (4–20 mmHg) versus right cardiac output. c) The relation between varying left afterload (MAoP) (60–120 mmHg) versus left cardiac output. d) The relation between varying right afterload (MPAP) (15–35 mmHg) versus right cardiac output. e) Hybrid Heart's reaction to left-to-right preload imbalance of -12 mmHg. f) Hybrid Heart's reaction to right-to-left preload imbalance of -12 mmHg.

biocompatible coating, and implantable driving system. Prior to the animal trial, we conducted an in vitro experiment against physiological pressures using the exact same prototype for more than two hours (>7000 cycles), to ensure its durability within the time range of an acute animal experiment. During open-heart surgery, we placed the goat on cardiopulmonary bypass. After removal of the native goat's ventricles, we surgically implanted the Hybrid Heart in the pericardial space. After de-airing and weaning from cardiopulmonary bypass, the Hybrid Heart was fully responsible for all blood flow in the goat during a 50 min testing period. We actuated the Hybrid Heart at 65 bpm, and we obtained 2.275 ± 0.035 L/min of cardiac output on both the left and right ventricles (average stroke volume 35 ml) (Fig. 4). Throughout the testing period, we recorded a mean aortic pressure of 49 mmHg and a mean pulmonary artery pressure of 17 mmHg from the data of two pressure sensors in the ascending aorta and the pulmonary artery. An additional pressure sensor in the iliac artery recorded systemic blood pressures between 70/35 mmHg and 105/46 mmHg (Fig. 4). After 50 minutes we had to stop the experiment due to a leakage in the pneumatic septum. The leakage was because of the delamination between TPU (inner layer) and nylon (outer layer) at the heat-sealing line.

Biocompatible coating

The biocompatibility of the blood-contacting surfaces of the Hybrid Heart was achieved by functionalizing a polycaprolactone bisurea (PCL-BU) coating with heparin to create an anti-thrombogenic surface. To bind heparin onto the TPU-coated nylon material, a heparin binding peptide was added to the system through coupling to a bisurea linker

(BU-HBP) allowing incorporation into the bisurea stacks formed in the system (Fig. 5a, b). Incorporation of 20 mol% of BU-HBP in the supramolecular coatings showed a reduction in water contact angle (Fig. 5c). This increased hydrophilicity was expected because of the polar amine side chains and amide bonds of the BU-HBP molecule. To evaluate the heparin binding to these surfaces, they were incubated in a solution containing heparin coupled with fluorescein isothiocyanate dye for 2 hours. When the BU-HBP concentration was increased to 20 mol%, the fluorescence intensity of the solution dropped (Fig. 5d), which indicated that heparin-FITC had specifically adsorbed to this coating.

24 hour testing with human umbilical vascular endothelial cells showed no cytotoxicity of the raw PCL-BU material, nor of the PCL-BU + BU-HBP coating (Fig. 5e) Thereafter, the anti-thrombogenic properties of the heparin functionalized coatings were investigated by incubating the materials with human blood plasma for 60 min and scanning electron microscopy analysis afterwards. On the uncoated TPU-coated nylon material, large platelet aggregates were observed. The TPU-coated nylon with a heparin-functionalized PCL-BU + BU-HBP coating, led to a reduction in platelet adhesion (Fig. 5f). Secondly, we assessed the biocompatibility of the supramolecular coatings on the TPU-coated nylon base material during an in vivo trial in rats (Fig. 6). We fabricated vascular grafts from TPU-coated nylon that we implanted as interposition grafts in the rat abdominal aorta ($n = 20$) (Figs. 6a, b, c, and S18). The rats were randomly allocated to the experimental groups. The investigators were blinded to group allocation during data analysis. By comparing the biocompatibility of vascular grafts made from i) uncoated TPU-coated nylon, ii) TPU-coated nylon coated with PCL-BU or with PCL-BU + BU-HBP (without heparin), and iii)
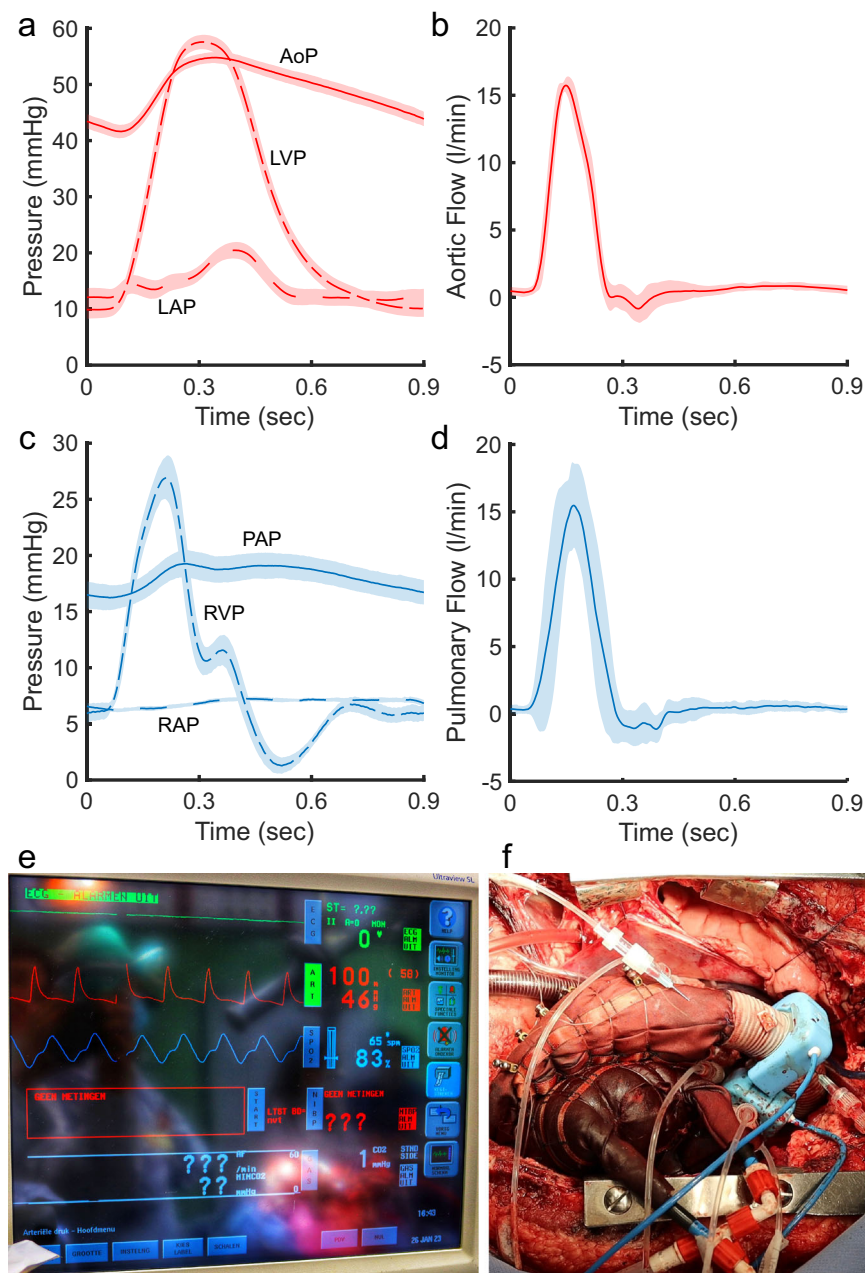
Fig. 4 | Test results of the Hybrid Heart in vivo experiment in an acute goat experiment. All data corresponds to the period during which the Hybrid Heart was providing all the blood flow in the animal, without additional support of the cardiopulmonary bypass. Data are presented as mean ± SD of $n = 20$ cycles with shaded error bars. **a** Systemic pressures measured during the in vivo experiment. AOP: aortic pressure, LVP: intra ventricular pressure of the left ventricle, LAP: left atrial pressure. **b** Aortic flow during the animal experiment. **c** Pressures of the pulmonary circulation measured during the animal experiment. PAP: pulmonary artery pressure, RVP: intra ventricular pressure of the right ventricle, RAP: right atrial pressure. **d** Pulmonary flow during the acute goat experiment. **e** Screen capture of the monitor during the animal experiment. Red line shows the blood pressure measured in the iliac artery (100/46 mmHg, mean 58 mmHg). f) Photo of the Hybrid Heart implanted in the goat.

TPU-coated nylon coated with PCL-BU + BU-HBP functionalized with heparin, a high number of thrombotic incidents with the uncoated TPU-coated nylon grafts was observed (Fig. 6d). However, the addition of PCL-BU + BU-HBP + heparin as a coating showed positive results, with the majority of grafts remaining patent (Supplementary Figs. S19–23). These findings suggest that supramolecular coatings based on bisurea polymers modified with heparin via heparin-binding additives reduce the thrombogenicity of TPU-coated nylon.

To implement the supramolecular coating in the Hybrid Heart's ventricles, we coated its entire blood-contacting surface (TPU-side) with PCL-BU through solution-casting. We characterized, by means of chemical analysis, the TPU-coated nylon material's surface with the PCL-BU coating before and after conducting tests in the mock circulatory loop. We found that after conducting the experiments in the mock circulatory loop, the PCL-BU coating was still present on the inside of the ventricles (Table S4). This proves that the supramolecular coating is firmly attached to the Hybrid Heart ventricle even when exposed to flow hemodynamics simulating physiological conditions.

Fully implantable control system exploration
During all above-mentioned in vitro and in vivo experiments, the Hybrid Heart prototype was actuated using an open pneumatic system
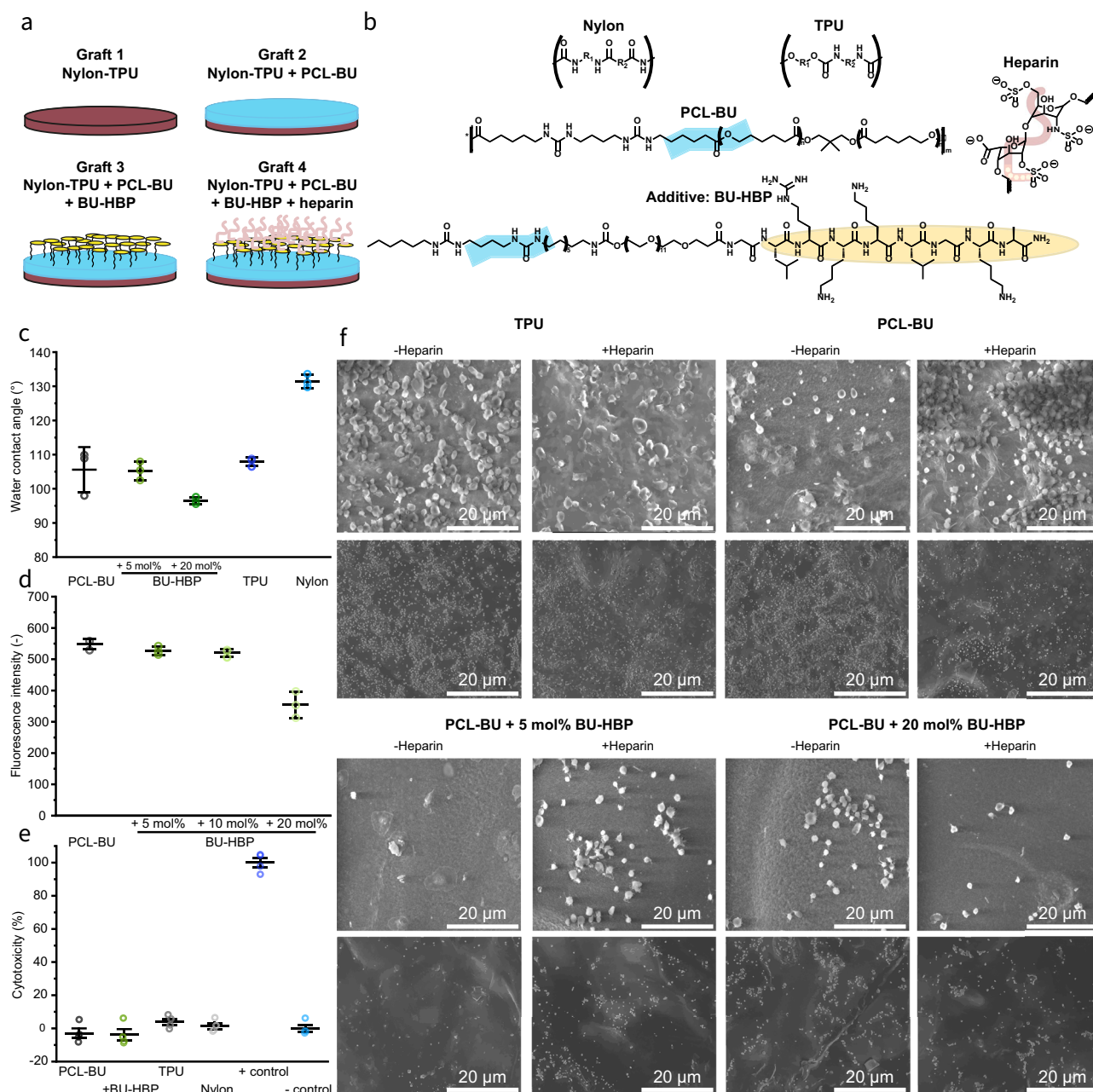
Fig. 5 | The biocompatible inner lining for the Hybrid Heart, in vitro studies on coated and uncoated TPU-coated nylon. a Schematic overview of the different grafts used in the in-vitro and in-vivo rat studies. **b** Chemical structures of Nylon, TPU, PCL-BU, heparin and BU-HBP. **c** water contact angles of TPU-coated nylon material with and without PCL-BU coating with or without 5 or 20 mol% BU-HBP. Data are presented as mean ± SD of $n = 3$ groups, each containing 3 samples. **d** Fluorescence of solution taken from TPU-coated nylon coated with PCL-BU with or without 5, 10 or 20 mol% BU-HBP. Data are presented as mean ± SD of $n = 3$ samples. **e** Cytotoxicity determined from LDH assay of TPU-coated nylon material with and without PCL-BU coating with or without 5 mol% BU-HBP. Data are presented as mean ± SD of $n = 4$ samples. **f** SEM images of platelets that adhered to the TPU-coated nylon materials with and without PCL-BU coating with or without 5 or 20 mol% BU-HBP either with heparin functionalization or without. We tested $n = 3$ samples for each material type, representative images are shown in this figure.

that is suitable for extracorporeal operation only. For future translation to the clinic, our objective is to develop a closed fluidic driving system, that is completely implantable. Towards this future driving system, we explored if it is possible to provide the required pressure profile to the Hybrid Heart's septum using a recently developed soft robotic actuation mechanism (including a hysteretic valve) that does not depend on electronics to generate a beating sequence[22]. This actuation system, the hysteretic valve, autonomously and passively transforms the constant flow provided by a continuous flow air pump into pressure pulses that generate the heartbeat for the Hybrid Heart (Fig. 7a). This method greatly simplifies the driving system and reduces

the number of failure-prone components such as electromechanical valves. The envisioned total pneumatic driving system consists of an implanted continuous flow air pump, an air container, and a soft hysteretic valve, connected to the septum in a closed circulation (Fig. 7c, and Video 4).

By furthermore integrating the closed fluidic system to a transcutaneous energy transfer (TET) system, the electrical energy to the pump is provided wirelessly, eliminating the need for external drivelines (Figs. 7c, S16). An external battery or power supply powers the external coil of the TET system, that is placed on the patient's skin. The external TET coil generates an electromagnetic field which transmits
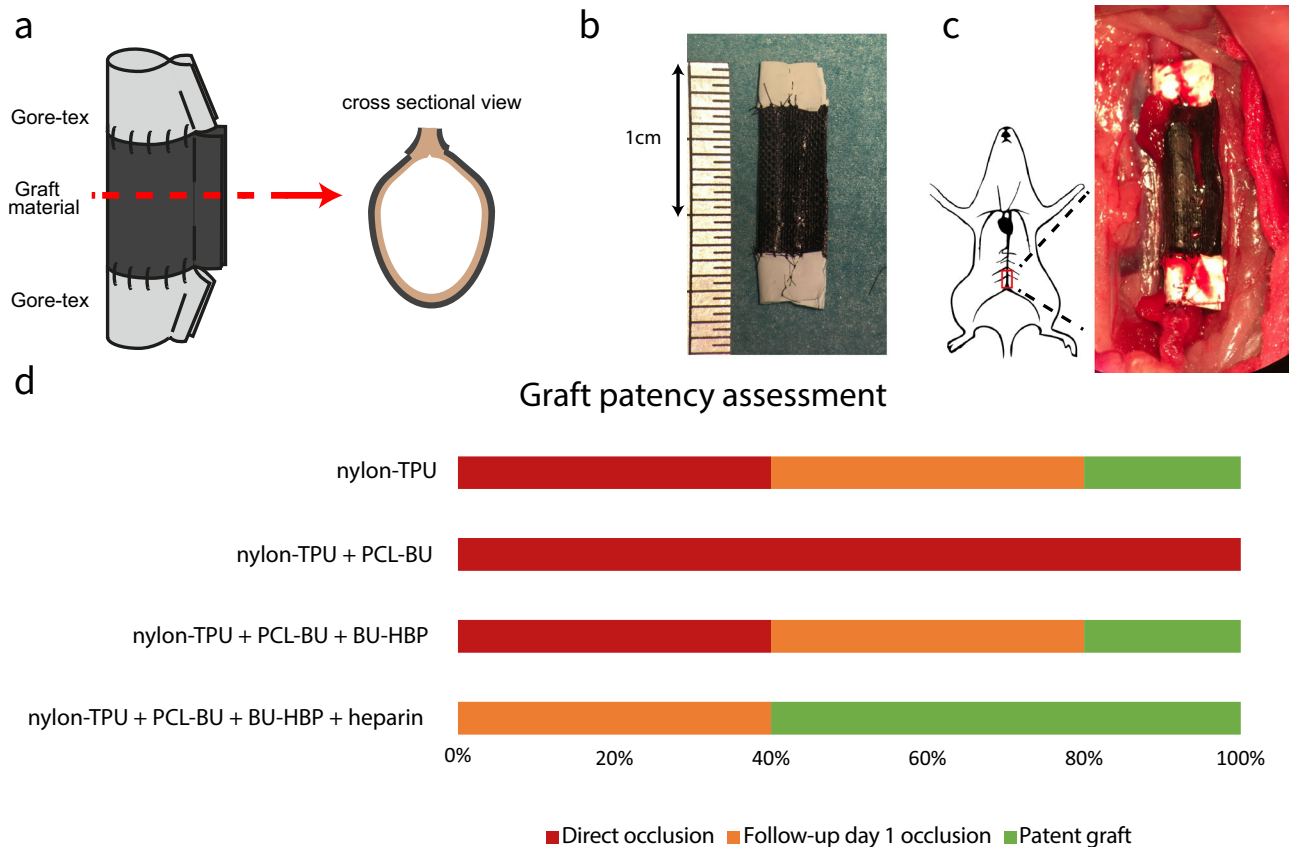
Fig. 6 | Pre-clinical assessment of the grafts. a Schematic drawing of the graft design with cross-sectional view as well. **b** Picture of fabricated graft. **c** Picture of implanted graft in rat aorta. **d** Assessment of the grafts in terms of occlusion based on hind leg movement and explantation.

power to the subcutaneously implanted internal TET coil, while leaving the skin intact. The internally implanted controller provides a stable output voltage to the implanted continuous flow air pump and the implantable battery packs. This approach reduces the risk of infection and enhances quality of life, as it allows future patients to temporarily detach from a power source and freely engage in activities like showering or swimming.

We performed an initial integration experiment to demonstrate the feasibility of this powering and actuation concept. In this experiment we used a TET system to transfer power to a continuous flow air pump connected to a closed fluidic circuit, that actuated the Hybrid Heart connected to the mock circulatory loop (Figs. 7c, and S17). Upon powering the continuous flow air pump, the Hybrid Heart automatically starts to beat at a heart rate of 35 bpm. The beat rate and applied pressure profile are not real-time controlled, but resulted from the air chamber, septum, and hysteretic valve properties. In this particular configuration, it provides a left stroke volume of 31 mL against a mean afterload of 66 mmHg, and a right stroke volume of 59 mL against a mean afterload of 12 mmHg. The difference in cardiac output is compensated by a shunt connected between the left and right pre-load chambers. Importantly, by varying the power supplied to the continuous flow air pump, we can modulate the cardiac output while the system is running, enabling periodic tuning or even real-time feedback control in the future. Note that pump speed mainly affects heart rate, not stroke volume (Fig. 7b). While these results demonstrate the concept, it should be mentioned that the cardiac output is still low. That is because in this initial experiment, compared to the traditional driving system, we are limited by the available power provided by the TET system. This is not a limitation of the TET system as such, nor a limitation of the valve and fluidic circuit itself, as higher input energy will result in a higher cardiac output (Fig. 7b). Therefore, we aim to

improve the energy efficiency of the control system in combination with the Hybrid Heart in the future.

Discussion

We are on the brink of a new era in which soft robotic technologies are making significant advancements. We present the first evidence that soft robotic techniques can be successfully utilized to create a TAH capable of delivering adequate cardiac output under physiological hemodynamic conditions in vitro, and can be successfully, though for now still with subphysiological performance, implanted and actuated in the acute animal model.

Our research has shown that the arrangement of wires, including their number and length, has impact on the ventricular performance, thereby making this technology potentially applicable to patients with various pathologies (Table S1). For instance, patients with pulmonary hypertension could benefit from wire adjustments to the right ventricle, that allow the right ventricular contractile force to be equal or even outperform the force of the left ventricle to overcome the pathological high pressures in the pulmonary circulation. Indeed, further studies are essential to characterize the effect of wire configuration (number, length, and position) on the cardiac output, which enable us to create a more robust design and utilize this adjustability as a solution for patients with different pathologies.

On itself, the Hybrid Heart shows preload sensitive behavior due to its geometry, varying from 0.0510 to 0.550 L/min/mmHg (0.176 ± 0.213 L/min/mmHg) at different preloads (Fig. 3a, b), which is somewhat lower than the values reported for native human heart varying from 0.213 to 0.241 L/min/mmHg[23,24]. Regarding afterload sensitivity, comparing the right and left side, for a mmHg increase in the arterial pressure, right CO reduction is 3 to 4 times more than the reduction in left CO (Figs. 3c, d), which is comparable with human
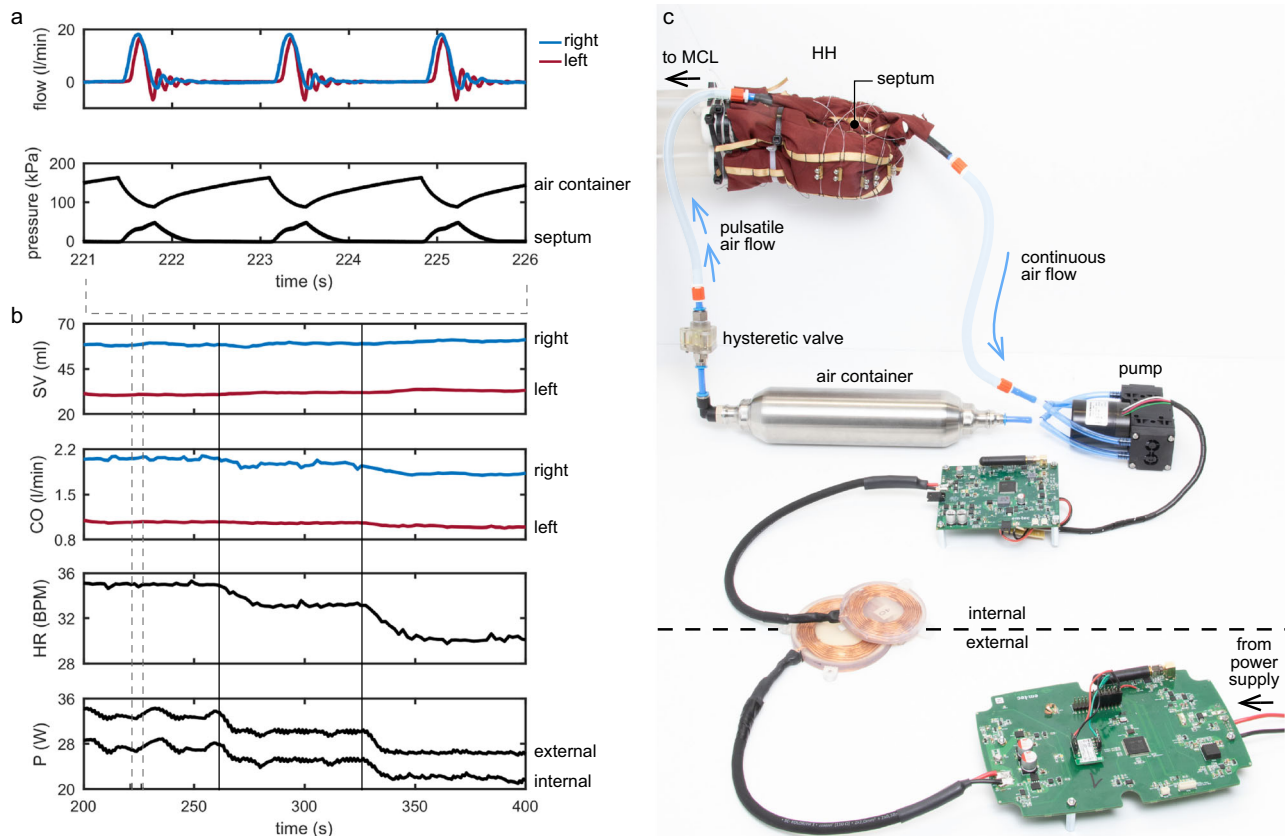
Fig. 7 | Integration test with implantable control system. a Left and right ventricular output flow (top panel) as a result of pressure pulses provided to the septum (bottom panel). **b** (all panels show 10-beat moving average values). Two vertical solid lines indicate two instances where input power is manually decreased to demonstrate the effect of electrical input power on hybrid heart output. SV = stroke volume, CO = cardiac output, HR = heart rate, P = electrical power.

c Components of the experimental setup, showing how the septum of Hybrid Heart (HH) is connected inline with the sealed air circulation of the implantable control system. The ventricles of the Hybrid Heart are connected to a mock circulatory loop. A horizontal dashed line demarcates the division between the internal and external components of the transcutaneous energy transfer (TET) system.

heart performance[24,25]. By developing and implementing additional mechanisms that enhance preload sensitivity, the Hybrid Heart will ultimately be able to adapt to a larger range of hemodynamic conditions, while maintaining balanced cardiac output at different conditions. One possible approach is the implementation of origami[26,27] folds in the ventricles to allow for additional buffer volume for increased venous returns, while keeping the end systolic volume constant. Such origami folds may also positively affect blood-material interactions, similar to corrugations in the endocardium arterial lumen[28]. These adjustments may also be tailored to the patient's specific needs. For example, patients with a large bronchopulmonary shunt flow may benefit from extra buffer volume in the left ventricle. Another benefit of soft artificial hearts in general, is that the patient may be resuscitated via chest compressions until the patient is connected to extracorporeal membrane oxygenation (ECMO), in case of an acute emergency. This is impossible with the currently available LVADs and TAHs.

Balancing left and right ventricular outputs in a TAH is challenging due to dynamic hemodynamic changes and the higher afterload on the left ventricle, which limits its stroke volume. Failure to maintain this balance can result in severe complications, such as lung edema and respiratory failure, which are common causes of death in chronic animal trials with TAHs[29]. Existing TAH designs use various methods to achieve balanced output, including compliant ventricular materials, passive shunts, active control mechanisms, and size adjustments of the right ventricle[29], among which Passive preload-sensitive mechanisms offer advantages over sensor-based systems, which are prone to

malfunctions[8]. Our studies illustrates that the Hybrid Heart is able to provide balanced output by adjusting the wire length around each ventricle, and due to its preload sensitivity, it can inherently balance the output in case of any acute changes in the system (Fig. 3e, f). However, we are aware that it is still limited to a few conditions and can probably not cover all possible condition that may happen in the human body. Therefore, our aim for future studies is to identify, explore, and employ the inherent properties of soft materials and structures for passive ventricular filling and output regulation, leading to a sensorless and robust system.

To enhance its biocompatibility, we introduced the concept of a Hybrid Heart by combining soft robotics that deliver contraction, with supramolecular coatings that are modular and have the potential for dual functionalization to combine anti-thrombogenic properties while stimulating endogenous endothelialization through in situ tissue engineering to ensure long-term hemocompatibility, potentially without the long-term use of anti-coagulants. These materials allow for the incorporation of functional additives, such as peptides or extra cellular matrix derived molecules through a mix-and-match approach[30,31]. Such biomaterials have proven suitable for in situ tissue engineering in clinical and large animal trials for cardiovascular applications such as heart valves[32–34], vascular grafts[35] and cardiac patches[36], which also proves their scalability to larger models. These cell-free constructs made from biomaterials are designed to induce regeneration upon implantation, directly at the functional site[37]. Our proof-of-concept in vitro and in vivo (rat) experiments show that supramolecular coatings can potentially be used to

improve the biocompatibility of the blood contacting surfaces of the Hybrid Heart.

The presence of folds may be an important finding for further optimization of the supramolecular coatings to grow an endothelial monolayer, as folds have been suggested as mechanostructural cues to modulate cell fate and the initial infiltration of immune cells (such as neutrophils) upon implantation in vivo[38]. Future research, by means of e.g., computational fluid dynamics (CFD)-CT, needs to assess if these folds result in blood stasis or not. The native human heart also has folds on the inside that probably are at the same location at every heart cycle and do not result in stasis of blood; usually blood stasis only occurs in areas with no contractility (e.g., ventricular aneurysm following myocardial infarction). To further enhance the biocompatibility of the Hybrid Heart, a coating that promotes the recruitment of host cells to initiate endogenous colonization of the ventricular surfaces, ultimately forming a functional endothelial monolayer[39] could be used. Previously, we have found that the binding of endothelial cells to supramolecular materials can be further improved through functionalization with vascular endothelial growth factor (VEGF)[39]. A next step is to translate the cell-binding properties to the BU supramolecular system, that is used for the coating of the Hybrid Heart's ventricles. Ultimately, the potential dual activity of the Hybrid Heart's blood-contacting surfaces will be investigated, both as an anti-thrombogenic surface (e.g., heparin) and as an inducer of endothelial monolayer formation (e.g., VEGF).

Use of a TET system reduces the risk of infection and enhances quality of life, as it allows patients to temporarily detach from a power source and freely engage in activities like showering or swimming. We aim to improve the energy transfer of the actuator to the blood, redesign the architecture of the fluidic circuit, and develop pneumatic pumps specifically designed for the hybrid heart. By further optimizing the integral system design, we aim to achieve an efficiency, such that the system can provide sufficient cardiac output using 25 W of electrical energy, the power that our TET system can continuously supply.

This research represents a collaborative effort across multiple disciplines, establishing a platform that facilitates future investigations. Though, it is important to note that all ingredients together still have to be tested in (chronic) large animal studies.

In conclusion, soft robotics technology can be a game-changer in developing TAHs by enabling biomimicry designs that have the potential to evolve into more efficient, biocompatible and blood friendly devices. This paper presents the first proof-of-concept of a soft, biocompatible TAH and, as such, creates a new horizon in the treatment of heart failure and transplantation medicine that is not currently available or anticipated.

Limitations and future perspective

It is important to note that this study presents a first important step in bridging several fields, yet all ingredients together still have to be improved and tested in animal studies. For practical reasons, we did not use medical-grade materials yet. The material used here for prototyping the ventricles and the septum (TPU-coated nylon) was chosen for its cost-effectiveness and ease of use. Moreover, the heat-sealing technique is also utilized only as a fast-prototyping method that enable us fabricate and test the samples easier and faster for further improvements. Future studies will be performed on developing and evaluating new fabrication methods employing durable and biocompatible materials.

Since the Hybrid Heart is soft, it is crucial to consider the interaction between the device and its surrounding organs after implantation and how the device responds in different conditions. This includes some optimizations on its size, design, and also anatomical shape. Moreover, the whole device including the full fluidic circuit, electronics and the TET system are not yet fully implantable. Future studies and developments are needed to assess and increase energy efficiency

of the system, by which we hope to minimize the size of the whole system and bring it closer to a fully implantable device.

In this study, pneumatic actuation was selected for in vitro experiments due to its simplicity and ease of use. However, it is not an ideal long-term solution, as it poses safety concerns and limits device controllability. Additionally, air compressibility restricts the device from providing higher outputs at higher frequencies, as we observed that the cardiac output starts to decline after reaching a certain beating rate (Supplementary Fig. S10). To overcome these limitations, future research should focus on developing a hydraulic septum and actuation system, enabling more precise volume-controlled experiments both in vitro and in vivo. It should be noted that the Hybrid Heart already demonstrates a very limited effect of heart rate on afterload sensitivity (Fig. 3c, d), suggesting the potential for a simpler control system.

Methods

Design and fabrication

We customized a CNC machine (Felix Tec4, FELIXprinters, Ijsselstein, The Netherlands) to heat-seal two layers of TPU-coated nylon together using a specific pattern designed in a 2D design software (Adobe Illustrator, Adobe, California, United States) (Supplementary Figs. S1a, S1b). We then inserted the TPU-coated nylon ventricles and septum (Fig. S1c) into a polyester fabric sleeve that is used to guide the wires and keep them in plane (Fig. S2). Multiple inextensible wires (100% Fluorocarbon, 0.46 mm, SavageGear, Gadstrup, Denmark), wrapped around the septum and ventricles in a closed-loop infinity symbol (∞), distribute the forces over the surfaces of both ventricles of the Hybrid Heart (Fig. 2). We used four mechanical valve prostheses (Sorin Bicarbon, Sorin Group, Milan, Italy) as inflow and outflow valves with diameters of 21 mm and 27 mm, respectively.

Actuation method for in vitro and in vivo experiments

The septum is inflated to induce systole and then deflated to create diastole. For driving the septum in the mock circulatory loop and the in vivo experiments (Supplementary Fig. S15), two digital solenoid valves (MHE2-MS1H-5/2-QS-4-K, Festo, Esslingen am Neckar, Germany) connect the septum to either pressurized air or vacuum. By controlling the opening and closing of the solenoid valves, we are able to adjust the beat rate and also the systole and diastole timing to explore and investigate the working behavior of Hybrid Heart under different conditions. The air pressure is set by a digital pressure regulator (VEAB-L-26-D18-Q4-V1-1R1, Festo, Esslingen am Neckar, Germany). The vacuum is generated continuously, using a vacuum generator (VN-14-L-T4-PQ2- VQ3-RO2, Festo, Esslingen am Neckar, Germany). The maximum pressure inside the septum can be set according to the preference and is normally in the range of 70 to 100 kPa.

Quasi-static in vitro experiments

In the experiments to determine the mechanical characteristics of the Hybrid Heart, we measure pressures in each of the chambers directly with a pressure sensor (MPX5100DP, NXP, Eindhoven, The Netherlands). Concurrently, we measure bidirectional flow into and out of each of the chambers and integrate to obtain volumes. To measure flow, we place custom-built restrictions in line with the air connections to the chamber and we measure the pressure drop over these restrictions to obtain standard flow rates. In a separate experiment we calibrated the pressure drop over the restrictions against known standard flow rates produced by a mass flow controller (SLA5850, Brooks Instrument, Hatfield, Pennsylvania, USA), at various absolute pressures.

In all quasi-static in vitro experiments, we pressurize the left and right ventricle with pressure controllers (VEAB-L-26-D13-Q4-V1-1R1, Festo, Esslingen am Neckar, Germany), each set to its individual setpoint pressure. Then, in pressure-controlled experiments, we cycle

Table 1 | Parameter values, set in mock circulatory loop for characterization of Hybrid Heart's preload and afterload sensitivity

Parameter	Unit	Value
MAP	mmHg	60, 80, 100, 120
PAP	mmHg	15, 20, 25, 30
AP	mmHg	4, 6, 8, 10, 12, 14, 16, 18, 20
Heart rate	BPM	50, 60, 70, 80
Systole/diastole timing	_	~1/2

septum pressure (using a third pressure controller (same type as for the ventricles). We first pressurize the ventricles and let them settle for 30 s. Then, we increase the septum pressure from 0 to 80 kPa in 20 s, we hold the septum pressure for 15 s, and decrease from 80 kPa to 0 in 20 s, while monitoring all pressures and volumes.

In volume-controlled experiments, we use a mass-flow controller (MFC) (SLA5850, Brooks Instrument, Hatfield, Pennsylvania, USA) to inflate the septum at a controlled (quasi-static) rate of 0.2 SLPM (standard liter per minute). Thereto, we connect the outflow of the MFC to the septum via a solenoid-operated three-way valve. To deflate the septum, we connect a restriction (918050-TE, Metcal, Menlo Park, CA, USA) to the septum via a solenoid-operated two-way valve. We turn on the MFC at the desired flow rate and let the flow stabilize, while the three-way valve is set to vent the air to the surroundings. Then, we switch the valve so that the air inflates the septum. After 50 s, we switch the three-way valve to its initial position, to stop inflow. After another 5 s, we switch the two-way valve, such that the septum deflates, for 100 s.

Evaluating the dynamical behavior of the hybrid heart
Mock circulation loop. Our double mock circulatory loop (Supplementary Fig. S11, S12) can mimic various systemic and pulmonary afterloads and preloads, as well as systemic and pulmonary peripheral resistances and compliances. The pulmonary and systemic arterial circulations (afterloads) are both simulated using a two-element Windkessel containing a compliance chamber followed by an adjustable resistance valve (Type 3232 2/2 way diaphragm valve, Burkert, Ingelfingen, Germany). These afterload chambers are sealed with a lid, and the compliance can be adjusted by altering the water level in the chamber. The resistor valves are manually adjustable and are used to simulate vascular resistance (for pulmonary and systemic sides separately). Venous compliances and preloads are simulated using an open-to-air chamber for right and left side separately, in which the water level can be altered. All preload and afterload pressures are measured by electronic pressure sensors in each compliance chamber (XMLP500MC11F, Schneider Electric, Rueil-Malmaison, France). Left and right cardiac output were measured using two ultrasonic clamps on liquid flow sensors (DIGIFLOW-EXT1, Emtec, Finning, Germany). In vitro testing has been conducted with 40% glycerol solution in tap water, as well as with 100% tap water.

Actuation method. The septum is pneumatically actuated in a pulsatile manner using a digital pressure controller (VPPE-3-1-1/8-2-010-E1, Festo, Esslingen am Neckar, Germany). Inflation of the septum induces systole, while deflation creates diastole, with the heart rate determined by the timing of these phases. To drive the septum, two digital solenoid valves (MHE2-MS1H-5/2-QS-4-K, Festo, Esslingen am Neckar, Germany) alternately connect it to a pressure tank with regulated pressurized air or a vacuum tank maintained at -10 kPa by a vacuum pump (VN-14-L-T4-PQ2-VQ3-RO2, Festo, Esslingen am Neckar, Germany). When connected to the pressurized air source, the septum inflates, and when linked to the vacuum tank, it deflates. By controlling the solenoid valves, both the beating frequency and the timing of

systolic and diastolic phases can be adjusted, allowing for the evaluation of the Hybrid Heart's performance under different conditions.

We calculated the average cardiac output by multiplying average stroke volume to beating rate. To determine the stroke volume, we measured the area under the flow curves, obtained from flow sensors that are placed after outlet valves right before the afterload chambers. To obtain the stroke volume, we conducted three separate experiments under identical conditions using the same prototype. From each experiment, we analyzed five random cycles selected from the regions where the device operated steadily. Therefore, the reported values for cardiac output are based on 15 cycles taken out from three separate experiments on same prototype.

To study the deformation of the ventricles during contraction in in vitro tests, we inserted a laparoscope (HOPKINS II 26003 BA, KARL STORZ, Tuttlingen, Germany) into the Hybrid Heart ventricles.

In vitro characterization of the Hybrid Heart's preload and afterload sensitivity
Table 1 specifies the parameter variations used for in vitro characterization of the Hybrid Heart's preload and afterload sensitivity, over which we have control using our mock circulation loop. These experiments were conducted in the same mock circulatory loop as mentioned above. The same actuation method was also used as explained above using an alternative vacuum pump (AMEB71-FY4R3N1Q4, AEG, Berlin, Germany). Mean aortic pressure (MAP) and pulmonary artery pressure (PAP) was used respectively to control systemic and pulmonary resistances. Different levels of afterload in the systemic and pulmonary circulation were achieved by manually adjusting the systemic and pulmonary resistance valves to maintain the reference MAP and mean PAP, as specified in Table 1. The left and right atrial pressures (AP) were held constant at 10 mm Hg for afterload sensitivity experiments. For preload sensitivity experiments, we kept the afterload constant to a mean AoP of 100 mmHg and a mean PAP of 25 mmHg. The preload was then changed by adding water to the preload chambers in steps of 2 mmHg, starting from 4 mmHg up to 20 mmHg.

For demonstrating the Hybrid Heart capability of balancing the cardiac outputs to compensate left and right preload difference, the imbalance between left and right preloads was created by using a roller pump (505S, WATSON MARLOW, Rotterdam, The Netherlands) on a shunt between the two preload chambers. The pump can displace water in both directions, causing pressure to rise in one chamber while simultaneously decreasing in the other. Therefore, in each experiment, consisting of a total of 200 cycles, the Hybrid Heart runs for a few initial cycles before activating the pump to displace water. The displacement occurs either from left to right preload (Fig. 3e) or from right to left preload (Fig. 3f). The initial mean AoP and PAP are set at 100 and 25 mmHg, respectively, and the preload is set at 10 mmHg on both sides. Once the pump is activated, it operates until the preload reaches ~16 mmHg in the increasing-preload chamber and 4 mmHg in the decreasing-preload chamber. At this point, the pump is turned off, and the system continues running until the experiment concludes. All data are recorded throughout the whole process and then analyzed cycle by cycle in MATLAB (R2024b, MathWorks).

In vivo experiment
For in vivo testing the acute goat model was used. The goat is a frequently used animal model for TAH testing[8,40,41]. The body weight and hemodynamics of large adult goats are comparable to those of humans[42–44]. In addition, the hemodynamics of a large adult goat does not change over time, as the adult goat does not grow. This is a clear advance over the use of calves as animal model for long term trials, where the growth of calves leads to increasing cardiac demands during the follow-up period. First, we tested the device prototype in mock circulatory loop to confirm its performance. Thereafter, four

mechanical heart valves were sutured in a continuous fashion to the TPU-coated nylon inner layer and polyester outer layer (5–0 Prolene C1, Ethicon, Somerville, US). We used 19 mm mechanical outflow valves and 25 mm mechanical inflow valves (Sorin Bicarbon, Sorin Group, Milan, Italy). Woven vascular prostheses (22 mm diameter; Gelweave, Vascutek, Inchin- nan, United Kingdom) were sutured to the outflow valves for easy implantation to the native aorta and pulmonary artery. Atrial cuffs were fabricated using two Hemagard strips per cuff (Hemagard Carotid Patch 25 × 150mm; Getinge, Gotenburg, Sweden) and sutured to the mechanical inflow valves (Fig. S14). Approval for the animal studies was obtained by the Amsterdam University Medical Center's Animal Care Ethics Committee (AVD1180020209766) and was in agreement with the current Dutch law on animal experiments (WOD). In total 2 female Dutch white goats underwent acute implantation with our Hybrid Heart prototype, of which the second experiment is reported here. The first experiment was a try-out to practice the surgical procedure. For the reported acute experiment, we used a 2.5-year-old female white goat of 65 kg. We used propofol to induce anesthesia (2–4 mg/kg IV; propofol 20 mg/mL, Fresenius Kabi, Bad Homburg, Germany) and to maintain anesthesia (20 mg/kg/h IV) during surgery. We used sufentanil (5 mcg/kg/h IV, Sufentanil-Hameln 50 mcg/mL, Hameln, Gloucester, UK) as pain relief during surgery. We added a single dose of amiodarone hydrochlorine (300 mg IV, cordarone 50 mg/mL, Sanofi, Paris, France) in the saline infusion bag before starting cardiopulmonary bypass (CPB). The animal was placed in the dorsal position. A 25 Fr venous cannula (Maquet, Rastatt, Germany) was inserted in the left jugular vein following the Seldinger technique. A midline sternotomy was performed and the pericardium was opened. We placed a 20 Fr arterial cannula (Edwards Lifesciences, Irvine, US) in the ascending aorta and a 24 Fr venous cannula (Maquet, Rastatt, Germany) in the inferior caval vein. We placed the goat on CPB after heparinization (15000-20000IU IV, Heparine 5000IU/mL, LEO, Ballerup, Denmark). We used CPB flow rates between 4-4.5 L/min. An activated clotting time >400 seconds was maintained during CPB and arterial blood gas analyzes were performed. The animal was cooled down to 30 °C. The ascending aorta was clamped just proximal to the junction of the brachiocephalic trunk. We administered 455 mL of St Thomas' Hospital Cardioplegic Solution number 1 to arrest the heart. We excised the native ventricles, leaving a rim of ~2 cm of the ventricular wall from the mitral and tricuspid annulus in situ. The leaflets of the mitral valve and the tricuspid valve were excised. The native atria were kept intact. The TAH was first sutured to the atrioventricular junctions and then to the pulmonary artery and aorta, using continuous sutures (5-0 Prolene RB, Ethicon, Somerville, US) and carefully de-aired. The animal was rewarmed and the aorta clamp was removed. The TAH was actuated. During actuation of the TAH, the weaning from extracorporeal circulation was initiated until the extracorporeal circulation was stopped. Phenylephrine was administered intravenously as vasoconstrictive medication at an infusion rate of 1500–2500 µg/hour. The cardiac output of the TAH was measured by two ultrasonic flow sensors (MC24PAU and MC28PAU COnfidence Flowprobes, Transonic, Ithaca, New York, US) clamped on the vascular grafts to the aorta and pulmonary artery. We measured pressure in the aorta, pulmonary artery, left and right atrium, and inside the left and right ventricles. We left the chest of the goat open during the full length of the experiment. At the end of the experiment the animal was exsanguinated under full anesthesia, after which the implanted TAH was explanted.

Control system

To determine the performance of the Hybrid Heart when actuated by the soft robotic fluidic circuit and TET system (Fig. S16), we connected a high-performance membrane pump (NMP850.1.2KPDC-B4 HP, KNF Verder B.V., Utrecht, the Netherlands), a 400 mL air container (CRVZS-0.4, Festo, Esslingen am Neckar, Germany), and a hysteretic valve[22] in a 3D-printed holder, in a closed circulation with the septum, using PU tubing (PUN-H-6×1-BL, Festo, Esslingen am Neckar, Germany), silicone tubing (SFM3-4050, Trelleborg Healthcare and Medical, Trelleborg, Sweden) and Nordson connectors (MLRL035-1, FSLLR, FTLL035-1, Nordson Medical, Westlake, Ohio, USA) (Fig. S17). An external power supply was used to provide electrical power to the external electronics of the TET system. The external and internal coils were positioned with respect to each other using a 3D-printed holder and were separated by an air gap (6 mm air gap). The internal controller of the TET system conditioned the received electrical power and provided 17.5 V to the pump (NMP850.1.2KPDC-B4 HP, KNF Verder B.V., Utrecht, the Netherlands). A control voltage (Vctrl = 0–5 V) was supplied to the pump via a custom, manually adjustable power supply to set the target pump speed. The internal voltage, as well as the internal and external power were monitored with a sample rate of 1.2 Hz.

Biocompatible innerlining

In vitro tests. Polycaprolactone bisurea (PCL-BU), whose synthesis has been described previously[45], was dissolved with or without 5,10 or 20 mol% BU-HBP in 1,1,1,3,3,3-hexafluoro-2-propanol at a concentration of 20 mg/mL. Heparin functionalization of the materials was performed in 96-wells plates by incubating the materials with 100 µL of sterile heparin solution (100 mg/mL) for two hours and afterwards washing the samples twice in PBS prior to the experiments.

X-ray photoelectron spectroscopy (XPS) spectra were recorded to determine the atom composition of the supramolecular coatings on TPU-coated nylon with a Thermo Scientific K-Alpha spectrometer equipped with a 180° double-focusing hemispherical analyzer with a 128- channel detector.

For the Heparin FITC assay, 100 µL of Heparin-FITC (100 mg/mL) was added. The samples were incubated for two hours at 37 °C. Afterwards the solutions were removed from the samples and transferred to a new 96-wells plate. The fluorescence of this plate was measured with a fluorescence spectrometer using 495 nm excitation and 520 nm absorbance wavelength.

In vitro cell culture. Cytotoxicity assay was conducted using human umbilical vein endothelial cells (HUVECs, Lonza). HU- VECs were cultured in endothelial cell growth medium 2 (ECGM-2, PromoCell) supplemented with 2% (v/v) fetal calf serum (FCS, PromoCell), growth factors (ECGM- 2, bullet kit, PromoCell) and 1% (v/v) penicillin and streptomycin (P/S) (Gibco) in a humidified incubator at 37 °C and 5% CO2. HUVECs were used at passage 3, and medium was changed every 2–3 days, when cells were 90% confluent, they were detached using accutase (STEMCELL Technologies). Cells were seeded in 96 well plate at seeding density of 3×10^4 cells/cm2 and incubated in culture medium from different tested material as referred to later.

The cytoxicity of coated and uncoated TPU-coated nylon was determined using CyQUANT™ LDH Cytotoxicity Assay (Invitrogen, Thermo Fisher Scientific, Waltham, US) following the manufacturer protocol. The samples were placed in 96-wells plates and fixed in place with an O-ring on top. The samples were incubated in endothelial cell growth medium 2 (ECGM-2, PromoCell) supplemented with 2% (v/v) fetal calf serum (FCS, PromoCell), growth factors (ECGM-2, bullet kit, PromoCell) and 1% (v/v) penicillin and streptomycin (P/S) (Gibco) for 24 h at 37 °C. The next day this medium was removed and added to the HUVECs for 24 hours. The negative control of this experiment were HUVECs cultured according to a standard protocol. For the positive control groups (maximum death of cells), lysis buffer 1:10 was added to HUVECs for 45 minutes. The following day 50 µL from all experimental groups was transferred to a new 96-wells plate and 50 µL of the reaction mixture from the CyQUANT™ LDH Cytotoxicity Assay was added. These solutions were incubated for 30 minutes and terminated by adding stop solution. Absorbance of the solutions was measured at 490 and 680 nm. The absorbance reading at 490 was subtracted from

the reading at 680 to eliminate the background signal. The cytotoxicity percentage was calculated following the formula:

$$\%Cytotoxicity = \left[\frac{Compound - treated\ LDH\ activity - Spontaneous\ LDH\ activity}{Maximum\ LDH\ activity - Spontaneous\ LDH\ activity} \right] \times 100 \tag{1}$$

Platelet adhesion assay. Human peripheral blood buffy coats were obtained from healthy donors with informed consent (Sanquin, Nijmegen, The Netherlands). These buffy coats were centrifuged for 20 minutes at 200 g. The top layer, consisting of platelets-rich plasma (PRP), was collected for the platelet adhesion assay. All the material conditions were functionalized with heparin by incubating them with 100 μL of sterile heparin solution (100 mg/mL) for two hours at 37 °C. Afterwards the samples were washed twice with PBS. 100 μL of PRP was added to the samples and they were incubated under gentle shaking condition (50 RPM) for 1 h in a humidified incubator at 37 °C and 5% CO2. The solutions were removed from the samples, and they were washed three times with PBS. Next, the samples were fixated in 4% (v/v) formaldehyde for 15 minutes and washed with PBS.

Scanning electron microscopy (SEM) was used to provide an overview for platelet adhesion and morphology.

in vivo study in rats
Fabrication of the grafts. Rectangular pieces measuring 18×10 mm were manually cut for all three materials (1 uncoated TPU-coated nylon, 2 TPU-coated nylon + PCL-BU, and 3 TPU-coated nylon + PCLBU + BU-HBP). These rectangular pieces were folded and sutured together with interrupted sutures (8–0 Ethilon, Ethicon, Raritan, New Jersey), resulting in a 10 mm long graft with 2 mm internal diameter (Fig. 6a, b). To prevent transanastomotic cell ingrowth into the graft[46] and to facilitate the suturing to the native aorta, we added Goretex (Preclude 1PCM102, Gore Medical, Newark, Delaware) strips on both sides of the grafts. The grafts were sterilized with ethylene oxide (Synergy Health, Venlo, The Netherlands) after fabrication.

In vivo study. Every experiment involving animals, human participants, or clinical samples has been carried out following a protocol approved by an ethical commission. Approval for the animal studies was obtained by the Amsterdam University Medical Center's Animal Care Ethics Committee (AVD1180020209766) and is consistent with the current Dutch law on animal experimentation (WOD). In total, 22 male Sprague-Dawley rats were used with a mean weight of 386 (± 13) grams and a mean age of 105 (± 4) days. Rats were randomly allocated into four groups of N = 5 animals, while 2 rats were kept for potential replacements in case of deaths during surgery. The follow-up time was 24 h. No anticoagulant was given during the follow-up period.

For experimental groups 1-3, grafts were implanted as fabricated, without further functionalization or treatments (1. uncoated TPU-coated nylon, 2. TPU-coated nylon + PCL-BU, and 3. TPU-coated nylon + PCL-BU + BU-HBP). For experimental group 4, sterile TPU-coated nylon + PCL-BU + BU-HBP grafts were submerged in heparin solution (100 μg/ml, Heparin Sodium H4784-1G, Merck Group, Darmstadt, Germany), during 2 hours prior to implantation under sterile conditions. After 2 h, the grafts were flushed with sterile saline and implanted immediately thereafter. Animals were anesthetized using isoflurane gas (2.5 %/L). Buprenorphine (0.05 mg/kg SC; Temgesic 0.3 mg/ml, Chesterfield, Virginia) was administered as general analgesic and a mix of lidocaine (1 mg/kg SC; Lidocaine 20 mg/ml, Fresenius Kabi, Bad Homburg vor der Höhe, Germany) and levobupivacaine (1.5 mg/kg SC; Levobupivacaine 2.5 mg/ml, Fresenius Kabi) was given as local analgesic at the incision site. Midline laparotomy was performed, and the abdominal viscera were lateralized for exposure of the abdominal aorta and the inferior vena cava. All side branches of the segment of the

abdominal aorta between the renal arteries and the aortic bifurcation were ligated (8-0 silk suture, Ethicon, Raritan, New Jersey). Next, the abdominal aorta was occluded with microvascular clamps. The aorta was transected, and 1.5 cm of the native abdominal aorta was removed. The proximal and distal lumen of the aorta were flushed with heparin (10 IU, heparin 5000 IU/mL, LEO, Ballerup, Denmark) to remove any clots. The graft composite was sutured with end-to-end anastomosis at both the proximal and distal ends of the Gore-Tex sheets, using interrupted sutures (10–0 ethilon, Ethicon, Raritan, New Jersey). Afterwards, vascular clamps were removed, and the blood flow through the abdominal aorta was restored. The abdominal muscular layer was closed with running sutures (4–0 Vicryl, Ethicon, Raritan, New Jersey) and the skin was closed with intracutaneous running sutures (4–0 Monocryl, Ethicon, Raritan, New Jersey).

Assessments. When the rat had pale and cold hind legs that were not moving or dragging when walking after more than 1 hour after surgery, a human end point was reached and the rat was euthanized. To evaluate vessel patency, animals underwent in vivo MR imaging (MRI) at 24 h after implantation on a preclinical 7.0 T MRI scanner (MR Solutions, Guildford, UK) under full anesthesia (3% isoflurane in medical air). Due to unforeseen technical issues with the MRI scanner during the course of our studies, we could not make all planned MRI scans. We could only make MRI scans for n = 6 animals on POD1 (grafts 1.1, 1.2, 3.1, 3.4, 4.1, and 4.5). Furthermore, we obtained MRI scans for n = 3 animals on the same day of the surgery in animals that had to be killed early due to immobile hind legs after surgery (grafts 1.5, 2.3, and 3.5). For the remaining N = 11 rats, no MRI scan was taken.

After MRI scanning, the rats were transferred to the surgery table and the abdomen was opened under full anesthesia. The grafts were explanted, and the animals were sacrificed by exsanguination under full anesthesia. The grafts were cut in half and were fixated in 3.7% formalin for 24 h and washed in phosphate buffered saline (PBS).

Sections were stained for hematoxylin and eosin (H&E; HT1079 and HT110116, Sigma-Aldrich, Saint Louis, US).

Reporting summary
Further information on research design is available in the Nature Portfolio Reporting Summary linked to this article.

Data availability
All data supporting the findings of this study are available within the article and its supplementary files. Any additional requests for information can be directed to, and will be fulfilled by the corresponding authors. Source data are provided with this paper.

References
1. Bragazzi, N. L. et al. Burden of heart failure and underlying causes in 195 countries and territories from 1990 to 2017. *Eur. J. Preventive Cardiol.* **28**, 1682–1690 (2021).
2. Tatum, R., Briasoulis, A., Tchantchaleishvili, V. & Massey, H. T. Evaluation of donor heart for transplantation. *Heart Fail Rev.* **27**, 1819–1827 (2022).
3. Tsao, C. W. et al. Heart Disease and Stroke Statistics—2022 update: a report from the American Heart Association. *Circulation* **145**, e153–e639 (2022).
4. Dal Sasso, E., Bagno, A., Scuri, S. T. G., Gerosa, G. & Iop, L. The biocompatibility challenges in the total artificial heart evolution. *Annu Rev. Biomed. Eng.* **21**, 85–110 (2019).
5. Cianchetti, M., Laschi, C., Menciassi, A. & Dario, P. Biomedical applications of soft robotics. *Nat. Rev. Mater.* **3**, 143–153 (2018).
6. Aissaoui, N. et al. Understanding left ventricular assist devices. *Blood Purif.* **46**, 292–300 (2018).
7. Molina, E. J. et al. The society of thoracic surgeons intermacs 2020 annual report. *Ann. Thorac. Surg.* **111**, 778–792 (2021).

8. Vis, A. et al. The ongoing quest for the first total artificial heart as destination therapy. *Nat. Rev. Cardiol.* **19**, 813–828 (2022).

9. Gerosa, G., Scuri, S., Iop, L. & Torregrossa, G. Present and future perspectives on total artificial hearts. *Ann. Cardiothorac. Surg.* **3**, 595–602 (2014).

10. Moazami, N. et al. Does pulsatility matter in the era of continuous-flow blood pumps?. *J. Heart Lung Transpl.* **34**, 999–1004 (2015).

11. Cheng, A., Williamitis, C. A. & Slaughter, M. S. Comparison of continuous-flow and pulsatile-flow left ventricular assist devices: is there an advantage to pulsatility?. *Ann. Cardiothorac. Surg.* **3**, 573–581 (2014).

12. Roche, E. T. et al. A bioinspired soft actuated material. *Adv. Mater.* **26**, 1200–1206 (2014).

13. Zhang, J. et al. Robotic artificial muscles: current progress and future perspectives. *IEEE Trans. Robot.* **35**, 761–781 (2019).

14. Saleh, S., Liakopoulos, O. J. & Buckberg, G. D. The septal motor of biventricular function. *Eur. J. Cardiothorac. Surg.* **29**, S126–S138 (2006).

15. King, J. & Lowery, D. R. Physiology, cardiac output StatPearls [Internet], StatPearls Publishing, Treasure Island (FL) (2025).

16. Kumar, K. R. et al. in *Critical Heart Disease in Infants and Children* (Third Edition) 670 (eds Ungerleider, R. M.) 111–133 (Elsevier, 2019).

17. Guex, L. G. et al. Increased longevity and pumping performance of an injection molded soft total artificial heart. *Soft Robot* **8**, 588–593 (2021).

18. Roche, E. T. et al. Soft robotic sleeve supports heart function. *Sci. Transl. Med* **9**, eaaf3925 (2017).

19. Franklin, D. L., Van Citters, R. L. & Rushmer, R. F. Balance between right and left ventricular output. *Circ. Res.* **10**, 17–26 (1962).

20. Savarese, G. & Lund, L. H. Global public health burden of heart failure. *Card. Fail. Rev. 2017* **3**, 7–11 (2017).

21. Mamas, M. A. et al. Do patients have worse outcomes in heart failure than in cancer? A primary care-based cohort study with 10-year follow-up in Scotland. *Eur. J. Heart Fail* **19**, 1095–1104 (2017).

22. van Laake, L. C., de Vries, J., Malek Kani, S. & Overvelde, J. T. B. A fluidic relaxation oscillator for reprogrammable sequential actuation in soft robots. *Matter* **5**, 2898–2917 (2022).

23. Salamonsen, R. F., Mason, D. G. & Ayre, P. J. Response of rotary blood pumps to changes in preload and afterload at a fixed speed setting are unphysiological when compared with the natural heart. *Artif. Organs* **35**, E47–E53 (2011).

24. Hildebrand, S. et al. Controlling the flow balance: In vitro characterization of a pulsatile total artificial heart in preload and afterload sensitivity. *Artif. Organs* **46**, 71–82 (2022).

25. Pahuja, M. & Burkhoff, D. Right ventricular afterload sensitivity has been on my mind. *Circulation: Heart Fail.* **12**, e006345 (2019).

26. Ze, Q. et al. Soft robotic origami crawler. *Sci. Adv.* **8**, eabm7834 (2022).

27. Ou, J. et al. in *Proceedings of the 29th Annual Symposium on User Interface Software and Technology* 121–132 (Association for Computing Machinery, Tokyo, Japan, 2016).

28. Pocivavsek, L. et al. Active wrinkles to drive self-cleaning: A strategy for anti-thrombotic surfaces for vascular grafts. *Biomaterials* **192**, 226–234 (2019).

29. Gülcher, O. J., Vis, A., Peirlinck, M. & Kluin, J. Balancing the ventricular outputs of pulsatile total artificial hearts. *Artif. Organs* **47**, 1809–1817 (2023).

30. Dankers, P. Y., Harmsen, M. C., Brouwer, L. A., van Luyn, M. J. & Meijer, E. W. A modular and supramolecular approach to bioactive scaffolds for tissue engineering. *Nat. Mater.* **4**, 568–574 (2005).

31. Bonito, V. et al. Modulation of macrophage phenotype and protein secretion via heparin-IL-4 functionalized supramolecular elastomers. *Acta Biomaterialia* **71**, 247–260 (2018).

32. Kluin, J. et al. In situ heart valve tissue engineering using a bioresorbable elastomeric implant - From material design to 12 months follow-up in sheep. *Biomaterials* **125**, 101–117 (2017).

33. Mes, T. et al. Supramolecular polymer materials bring restorative heart valve therapy to patients. *Mater. Today* **52**, 175–187 (2022).

34. Morales, D. L. et al. A novel restorative pulmonary valve conduit: early outcomes of two clinical trials. *Front. Cardiovascular Med.* **7**, 583360 (2021).

35. Talacua, H. et al. Imaging the in vivo degradation of tissue engineering implants by use of supramolecular radiopaque biomaterials. *Macromol. Biosci.* **20**, 2000024 (2020).

36. Gu, X. et al. Sustained viral gene delivery from a micro-fibrous, elastomeric cardiac patch to the ischemic rat heart. *Biomaterials* **133**, 132–143 (2017).

37. Wissing, T. B., Bonito, V., Bouten, C. V. C. & Smits, A. I. P. M. Biomaterial-driven in situ cardiovascular tissue engineering—a multi-disciplinary perspective. *npj Regenerative Med.* **2**, 18 (2017).

38. Izawa, H. et al. Application of bio-based wrinkled surfaces as cell culture scaffolds. *Colloids Interfaces* **2**, 15 (2018).

39. Schmitz, M. G. J. et al. Heparin-guided binding of vascular endothelial growth factor to supramolecular biomaterial surfaces. *J. Polym. Sci.* **61**, 2524 (2023).

40. Mochizuki, S. et al. Results of animal experiments using an undulation pump total artificial heart: analysis of 10 day and 19 day survival. *Asaio J.* **46**, 500–504 (2000).

41. Abe, Y. et al. Results of animal experiments with the fourth model of the undulation pump total artificial heart. *Artif. Organs* **35**, 781–790 (2011).

42. Barszcz, K. et al. Topography of coronary arteries and their ramifications in the goat. *Biologia* **74**, 683–689 (2019).

43. Gumusalan, Y., Ozbag, D., Ozden, H., Saruhan, B. G. & Demirant, A. The comparative investigation of left ventricle papillary muscle arteries in different species. *Saudi Med J.* **27**, 826–832 (2006).

44. Li, M. et al. Physiological parameter values for physiologically based pharmacokinetic models in food-producing animals. part iii: sheep and goat. *J. Vet. Pharmacol. Therapeutics* **44**, 456–477 (2021).

45. Wisse, E. et al. Molecular recognition in poly(ε-caprolactone)-based thermoplastic elastomers. *Biomacromolecules* **7**, 3385–3395 (2006).

46. Talacua, H. et al. In situ tissue engineering of functional small-diameter blood vessels by host circulating cells only. *Tissue Eng. Part A* **21**, 2583–2594 (2015).

47. Willemet, M., Chowienczyk, P. & Alastruey, J. A database of virtual healthy subjects to assess the accuracy of foot-to-foot pulse wave velocities for estimation of aortic stiffness. *Am. J. Physiol. Heart Circ. Physiol.* **309**, H663–H675 (2015).

48. Wehrum, T. et al. Age dependence of pulmonary artery blood flow measured by 4D flow cardiovascular magnetic resonance: results of a population-based study. *J. Cardiovasc Magn. Reson* **18**, 31 (2016).

Acknowledgements

Author contributions

Conceptualization: M.A., A.V., J.K. Methodology: M.A., A.V., P.A.A.B., L.C.v.L., L.L., D.M.I., D.Z., A.I.P.M.S., A.H., M.C., P.Y.W.D., C.V.C.B., J.T.B.O., J.K. Investigation: M.A., A.V., P.A.A.B., L.C.v. L., L. L., D. M. I., D.Z., A.I.P.M.S., A.H., M.C., P.Y., W.D., C.V.C.B., J.T.B.O., J.K. Visualization: M.A., A.V., L.C.V.L, P.A.A.B., L.L., D.M.I. Funding acquisition: J.K. Project administration: J.K. Supervision: A.I.P.M.S., M.C., P.Y.W.D., C.V.C.B., J.T.B.O., J.K. Writing – original draft: M.A., A.V., L.C.V.L, P.A.A.B., L.L., D.M.I. Writing – review & editing: M.A., A.V., P.A.A.B., L.C.v.L., L.L., D.M.I., D.Z., A.I.P., M.S., A.H., M.C., P.Y., W.D., C.V.C.B., J.T., B.O., J.K.

Competing interests

The authors declare no conflict of interest.

Additional information

Supplementary information The online version contains supplementary material available at https://doi.org/10.1038/s41467-025-60372-6.

Correspondence and requests for materials should be addressed to Jolanda Kluin.

Peer review information *Nature Communications* thanks Ali Alazmani, and the other, anonymous, reviewer(s) for their contribution to the peer review of this work. A peer review file is available.

Reprints and permissions information is available at http://www.nature.com/reprints

Publisher's note Springer Nature remains neutral with regard to jurisdictional claims in published maps and institutional affiliations.